Sampling rare events in stochastic reaction-diffusion systems within trajectory looping

Pawel J. Zuk
Department of Biosystems and Soft Matter, Institute of Fundamental Technological Research, Polish Academy of Sciences, 02-106 Warsaw, Poland and Department of Mechanical and Aerospace Engineering, Princeton University, Princeton, New Jersey 08544, USA

Marek Kochańczyk and Tomasz Lipniacki*
Department of Biosystems and Soft Matter, Institute of Fundamental Technological Research, Polish Academy of Sciences, 02-106 Warsaw, Poland

(Received 28 May 2018; published 1 August 2018)

In bistable reaction–diffusion systems, transitions between stable states typically occur on timescales orders of magnitude longer than the chemical equilibration time. Estimation of transition rates within explicit Brownian dynamics simulations is computationally prohibitively costly. We present a method that exploits a single trajectory, generated by a prior simulation of diffusive motions of molecules, to sample chemical kinetic processes on timescales several orders of magnitude longer than the duration of the diffusive trajectory. In this approach, we "loop" the diffusive trajectory by transferring chemical states of the molecules from the last to the first time step of the trajectory. Trajectory looping can be applied to enhance sampling of rare events in biochemical systems in which the number of reacting molecules is constant, as in cellular signal transduction pathways. As an example, we consider a bistable system of autophosphorylating kinases, for which we calculate state-to-state transition rates and traveling wave velocities. We provide an open-source implementation of the method.

DOI: 10.1103/PhysRevE.98.022401

I. INTRODUCTION

Processes involving constituents that modify each other upon contact and diffuse in space arise in a multitude of fields as diverse as, e.g., geomorphology, population ecology, developmental biology, and, most naturally, (bio)chemistry. Such reaction–diffusion systems are often expressed and analyzed in terms of partial differential equations (PDEs) [1]. When molecular noise has a significant impact on the process of interest, a deterministic description in terms of PDEs becomes inappropriate and more fine-grained descriptions are necessary, such as stochastic simulations with a single-molecule resolution. However, molecular simulations of spatially extended systems are computationally demanding. When, in the chemical context, individual reacting molecules perform Brownian random walk in continuous space, the most compute-intensive part is finding and resolving their collisions. If hydrodynamic interactions are additionally taken into account, simulation of diffusive dynamics is particularly expensive [2]. Since typically molecules perform multiple random diffusive steps between collisions and only a fraction of collisions result in chemical reactions, the numerical cost of spatial stochastic simulations can be prohibitively high.

Computational analysis of oscillatory or multistable biochemical systems requires long simulation times to properly sample the phase space or collect multiple state-to-state transitions. Simulations of multistable reaction systems are demanding even in the well-mixed limit, when the efficient Gillespie algorithm [3] can be applied. To enhance sampling, reweighting-based [4] and importance sampling-based [5] approaches were developed in addition to metamethods, such as transition path sampling [6] or forward flux sampling [7], in which the Gillespie algorithm simulations can be framed. Such auxiliary rare event sampling schemes often turn out to be inevitable for the estimation of state-to-state transition rates and, in this way, for determining the relative stability of the steady states. Several approaches were devised to speed up spatial stochastic simulations by splitting the reaction and diffusion events, and treating the latter implicitly. For example, in the next subvolume (NSV) method [8], the reactor is decomposed into subreactors that are assumed to be well mixed whereas diffusion is included in the form of random transport of molecules between neighboring subreactors. Another approach that circumvents explicit simulation of Brownian motion, yet works at the single-molecule level, is the event-driven Green's function reaction dynamics (enhanced GFRD, eGFRD) [9,10]. In this approach, the spatial propagator displaces molecules directly to the locations where they react. One may accommodate chemical reactions within the direct simulation Monte Carlo method (DSMC), originally developed to simulate rarefied gases [11]. In DSMC it is assumed that each simulated molecule may represent a large number of actual molecules and that molecular motions (treated as ballistic, modeled deterministically) and intermolecular collisions (modeled stochastically) are uncoupled over small time intervals. The framework can be extended to account for disparate diffusivities of reacting molecules to study, e.g., formation of Turing patterns [12].

*tlipnia@ippt.pan.pl

Here we present "trajectory looping," a method that speeds up spatial stochastic simulations while still utilizing explicit simulations of Brownian motion of individual molecules. In the method we generate a trajectory of diffusive motions of the molecules and use it multiple times for sampling chemical processes on timescales that are several orders of magnitude longer than the simulated time of the original trajectory. The generated trajectory should be long enough to allow each molecule to form contacts with molecules other than its initial neighbors.

The proposed method is suitable for simulation of biochemical reactions in which substrate molecules are reversibly modified by enzymes, as often found in cellular signal transduction systems [13,14]. Crucially for the method, we assume that in the enzymatic reaction scheme: enzyme + substrate $\leftrightarrow$ enzyme–substrate complex $\rightarrow$ enzyme + product, the enzyme–substrate complexes are short-lived and thus the substrate can be modified instantaneously when in contact with the enzyme, according to the simplified reaction scheme: enzyme + substrate $\rightarrow$ enzyme + product. In such systems, the number of reacting molecules is constant.

We explain the algorithm, explore limitations, and test the accuracy of this approach applied to two systems of coupled biochemical reactions: a monostable phosphorylation–dephosphorylation cycle and a bistable reaction system of autophosphorylating kinases. We show for the latter system that the method enables estimation of the state-to-state transition rates as well as the speed of traveling wave propagation. Analysis of these processes requires simulations that last much longer than the reactor-scale Brownian time. These results are compared to results obtained with other methods.

II. RESULTS

A. Algorithm

A generic simulation workflow in which trajectory looping is embedded is presented in Fig. 1.

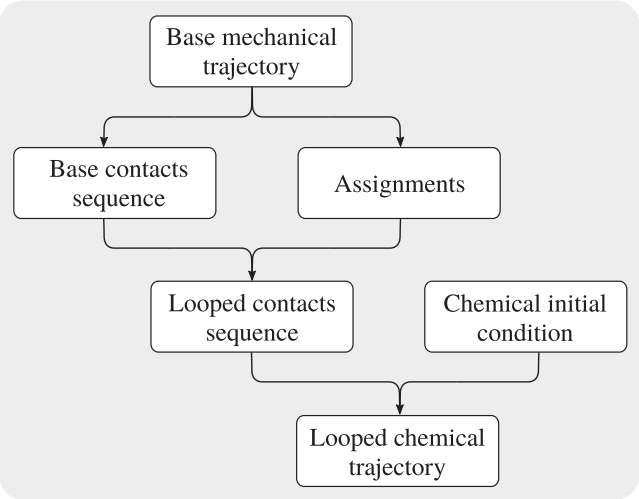

FIG. 1. Workflow for performing a chemical kinetic simulation of an arbitrary length by means of trajectory looping. An exemplary assignment is depicted in Fig. 2.

a. Base mechanical trajectory. Initially, one has to obtain a trajectory of N molecules represented by identical spheres of radius a, recorded at M equidistant time points separated by Δt. This trajectory, referred to as the *base mechanical trajectory*, should be obtained according to a scheme that generates molecule positions in a Markovian manner (that is, in a manner that is devoid of inertial effects). It is required that in each simulation step the positions of molecules are accordant with the equilibrium spatial distribution, guaranteeing that the neighborhoods of all molecules are statistically indistinguishable. For reasons that are explained further, the simulated system is expected to be translationally invariant which is achieved by imposing periodic boundary conditions in at least one spatial dimension.

The molecule-scale Brownian time τ_B that sets a natural time scale for the base mechanical trajectory is defined as the expected time required for a molecule to diffuse over its diameter $\tau_B = (2a)^2/D_0$, where D_0 is the diffusion coefficient of a molecule (in the absence of other molecules). All base mechanical trajectories subjected to looping and analyzed in this article were generated by performing standard Brownian dynamics simulations at a given volume fraction ϕ, as described in the Methods section.

b. Base contacts sequence. The only information contained in the base mechanical trajectory that is relevant to chemistry is that about molecule contacts. Two molecules are in contact when their center-to-center distance is smaller than the sum of their reaction radii. If reaction radii are identical for all molecules, being all equal $a + \delta/2$, then a significant simplification may be introduced: for each time step of the base mechanical trajectory a list of molecules of pairwise center-to-center distances smaller than the sum of reaction radii, $d_{ij} < 2a + \delta$, can be derived. Such a list of pairs of molecule indices, termed the *base contacts sequence*, is used as an input to the stochastic simulation of chemical events instead of the base mechanical trajectory.

c. Assignments. The base mechanical trajectory of duration $\theta = (M - 1) \times \Delta t$ is used to create a mechanical trajectory of length $\Theta > \theta$ by means of a (recursively applied) procedure that consists in joining the end of the base mechanical trajectory with its beginning and a subsequent molecule indices reassignment. To perform a join, one has to find an *assignment* in the form of a complete molecule-to-molecule index map that is used to transfer molecule identities (associated with chemical states) between molecules in the last time step and molecules in the first time step of the base mechanical trajectory. An optimal assignment that minimizes mean square displacements in pairs of corresponding molecules can be found in polynomial time, $\mathcal{O}(N^3)$, according to the Kuhn–Munkres algorithm [15,16] (also known as the Hungarian algorithm; in this article, we use an implementation from DLIB [17]). When performing consecutive joins, to prevent finding identical molecule-to-molecule assignments, one can make use of the translational invariance of the simulated system and, prior to finding pairs of corresponding molecules, apply a common random shift to all molecule coordinates along the direction(s) in which the system has periodic boundary conditions. For an exemplary assignment see Fig. 2.

d. Looped contacts sequence. Consecutive assignments are applied recursively to the base contacts sequence, yielding

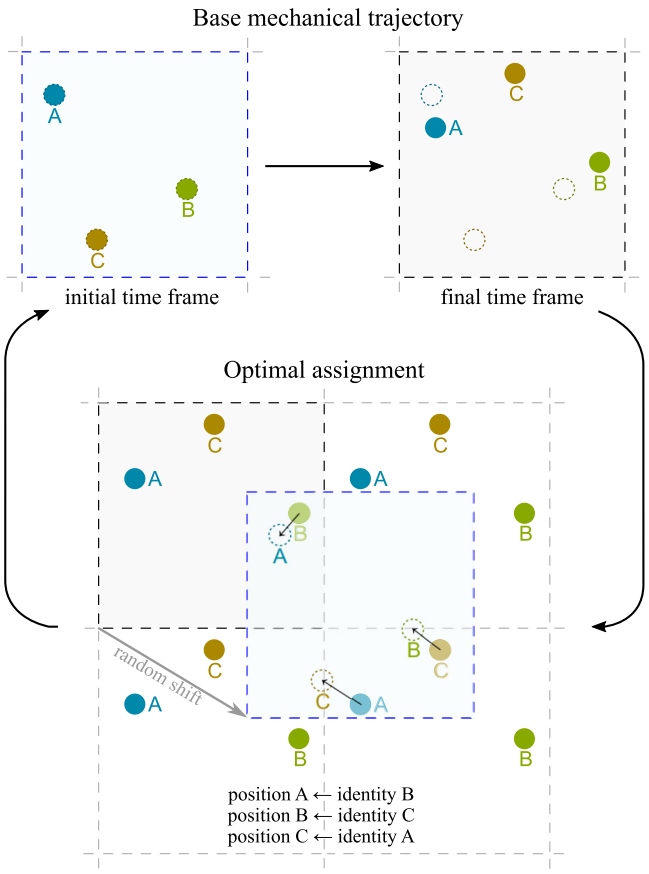

FIG. 2. An example assignment performed to join the end and the beginning of the base mechanical trajectory. Top: In the base mechanical trajectory, molecules (filled circles) depart from their initial positions (dashed circles) due to Brownian motion. The 2D simulation box has periodic boundary conditions in both directions. Bottom: To join the end and the beginning of the base mechanical trajectory, the initial time frame is randomly shifted in space (since periodic images of the final time frame are used, the initial time frame covers the total volume of the final time frame). Next, each molecule in the final time frame is uniquely mapped to a molecule in the initial time frame—in a manner that minimizes the sum of all square distances of molecules in such pairs—and then, according to the obtained index map, chemical identities of molecules in the final time frame of the base mechanical trajectory are transferred to corresponding molecules in the initial time frame.

the *looped contacts sequence*. The looped contacts sequence contains replicas of the base contacts sequence with molecules reindexed at each join. In this way, computationally expensive search of molecule contacts is performed once (for the base mechanical trajectory).

e. Chemical initial condition. Chemical states are assigned to every molecule in the first time step of the simulation; this assignment is called the *chemical initial condition*. It is assumed that all molecules have the same diffusivity and that their chemical state have no influence on their diffusion properties.

f. Looped chemical trajectory. In the course of the simulation, chemical states of molecules can be altered as a result of chemical reactions that are either unimolecular (i.e., first order) or bimolecular (i.e., second order). A unimolecular reaction may occur independently of the molecule neighborhood, whereas a bimolecular reaction may occur only when two molecules are in contact, i.e., when their center-to-center distance is smaller than the reaction distance, $d_{ij} < 2a + \delta$. No reaction is allowed to change the number of molecules in the system, N. In every time step within the looped contacts sequence, a complete list of possible reaction events is created. Time to a next reaction is drawn at random from exponential distribution with the expected value of the inverse of the sum of chemical rates of all events; reaction events are selected randomly from the complete list with probabilities that are proportional to respective rates. After a substrate is modified, new reaction events that are possible between the modified substrate and other molecules within reaction distance are added to the list. Stochastic simulation of reaction kinetics in a given time step of the looped contacts sequence proceeds as long as times to a next event lie within Δt.

The described event scheduling scheme constitutes an exact stochastic simulation method that for a sufficiently fast diffusion is consistent with the Gillespie algorithm [3] in which possible reactants are limited to molecules within the reaction distance. Since configurations of molecules in the base mechanical trajectory are in equilibrium, one can use the radial distribution function $g(\sigma|\phi)$, determined from the analytical solution of the Percus–Yevick integral equation for hard spheres [18], to count the expected number of molecules within the reaction distance:

$$\chi = \frac{N}{V} \times \int_{2a}^{2a+\delta} [g(\sigma|\phi) \times 4\pi\,\sigma^2] d\sigma.$$

To compare kinetics of our simulations with those obtained in the Gillespie simulations, bimolecular reaction rate constants for the latter method are multiplied by χ/N.

After K joins, a simulated record of chemical states of N molecules in $(K+1) \times M$ time steps will be referred to as the *looped chemical trajectory*. Trajectory looping performed multiple times enables recurrent trajectory reuse and simulation of chemical processes on timescales several orders of magnitude longer than the original diffusion trajectory.

Simulations of stochastic chemical kinetics within trajectory looping can be performed in our open-source software tool, LOOPER [19].

B. Limitations

Looped trajectories are distorted due to (*i*) displacements of molecules in end-to-begin joins and (*ii*) limited repertoire of single-molecule trajectories contained in the base mechanical trajectory.

a. Displacements of molecules in end-to-begin joins. In every end-to-begin join, each source molecule in the last time step of the base mechanical trajectory is assigned uniquely to a target molecule in the initial time step. A subsequent transfer of the "identity" of a source molecule to a target molecule causes an instantaneous molecule movement from the source to the target location [see kinks that appear every $n\theta = n\,10\tau_B$ in Fig. 3(a)]. The mean-square displacement (MSD) that results from such a join is $\langle r^2 \rangle_\phi^{\text{join}(k)} = \sum_{i=1}^{N}$

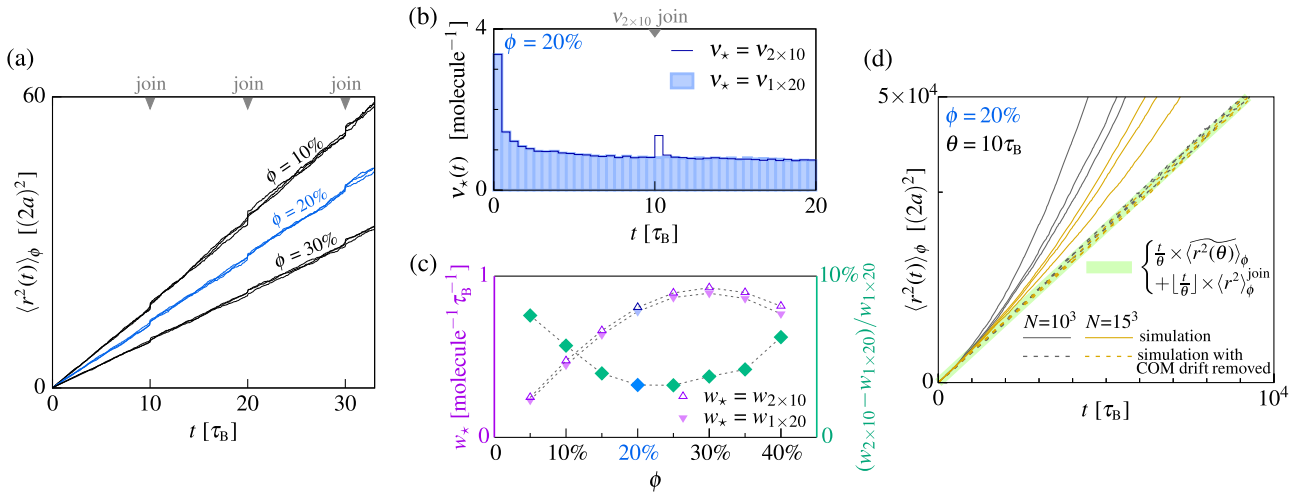

FIG. 3. Limitations of the trajectory looping method. (a) Mean-square displacement (MSD), denoted $\langle r^2(t)\rangle_\phi$, of molecules in trajectories subjected to looping, in the units of molecule diameter squared. Three independent trajectories are shown for each of three volume fractions, ϕ. Trajectories are joined every $\theta = 10\tau_B$. Sudden increase of MSD occurs upon joining. (b) Distribution ν of simulation times in which new molecule–molecule encounters are registered for two cases: the case of a single trajectory of duration $20\tau_B$, labeled "1×20," and for the case of a first half of that trajectory joined at $t = 10\tau_B$, labeled "2×10." Each distribution results from averaging the new encounter times obtained from five independent mechanical trajectories. Contact distance was set to $1.1\times2a$. (c) Number of new molecule–molecule encounters $w_\star$ calculated per τ_B in time range $[10\tau_B, 20\tau_B]$ in the trajectory with one end-to-begin join ($w_\star = w_{2\times10}$, open triangles) and in the nonjoined trajectory ($w_\star = w_{1\times20}$, filled triangles), and an excess of the new encounters in the trajectory with one end-to-begin join over new encounters in the nonjoined trajectory (diamonds). All w were calculated based on histograms obtained from five independent mechanical trajectories. (d) Faster than linear increase of MSD in time during $K = 10^3$ joins of the base mechanical trajectory of $\theta = 10\tau_B$ for two different system sizes N. For each N, MSD of three independent trajectories is shown. The displacement of the center of the mass (COM) in the base mechanical trajectory accumulates consistently upon looping, giving rise to the observed drift (solid lines). The COM drift is on average smaller for larger systems (orange vs. gray solid lines). When a trajectory-specific COM-related contribution to MSD is removed, such corrected MSD is linear (dashed lines) and agrees well with the expected linear long-time MSD (thick pale green line). In all panels, $\epsilon = 0.05$ (see Methods); in panels (a)–(c), $N = 1000$.

$|\vec{R}_{\sigma(k,i)}(0) - \vec{R}_{\sigma(k-1,i)}(\theta)|^2/N$, where $\sigma(k,i)$ denotes an index of an ith molecule in the base mechanical trajectory after k end-to-begin joins (initially $\sigma(0,i) := i$). Although the Hungarian algorithm is applied to minimize $\langle r^2\rangle_\phi^{\text{join}(k)}$, these displacements are still usually larger than the Brownian molecule displacements in Δt. The impact of distortions introduced by end-to-begin joins on the looped mechanical trajectory can be made relatively small when $\langle r^2\rangle_\phi^{\text{join}} \ll \langle r^2(\tau=\theta)\rangle_\phi$, where $\langle r^2\rangle_\phi^{\text{join}} = \sum_{k=1}^K \langle r^2\rangle_\phi^{\text{join}(k)}/K$, that is, for a sufficiently long base mechanical trajectory.

Molecule displacements in an end-to-begin join can significantly alter molecular neighborhoods. New molecule–molecule contacts can be formed at the expense of breaking existing contacts, which affects the looped contacts trajectory. To quantify this effect, we calculated a distribution of new encounter times in a trajectory of $\theta = 20\tau_B$ (without looping) and then a distribution of new encounter times after a first half of this trajectory was looped once [see Fig. 3(b)]. Encounters that are an artifact of looping are registered as an excess of the new encounters that peaks just after $10\tau_B$. At the assumed θ, the excess of the new encounters appears to be lower than 10% for volume fractions ϕ between 5% and 40% [see Fig. 3(c)].

b. Limited repertoire of single-molecule trajectories. If the optimal assignments were used to loop the base mechanical trajectory with explicit tracking of absolute positions of molecules, then one would obtain a *looped mechanical trajectory*. The base mechanical trajectory is just a single stochastic realization of diffusion of a finite set of molecules. A property that is specific to each base mechanical trajectory, and affects the apparent long-time MSD of molecules in the looped mechanical trajectory, is the displacement of the base mechanical trajectory center of the mass (COM) $\vec{\delta}_{\text{COM}}(\theta) = \sum_{i=1}^N [\vec{R}_i(\theta) - \vec{R}_i(0)]/N$. Generically, $\vec{\delta}_{\text{COM}}$ is a nonzero vector that due to looping adds to diffusive displacements of all molecules a contribution of direction and magnitude consistent among all end-to-begin trajectory joins. The expected value of $|\vec{\delta}_{\text{COM}}(\theta)|^2 =: \delta^2{}_{\text{COM}}(\theta)$ is proportional to θ and inversely proportional to N. If we define $\widetilde{\langle r^2(\theta)\rangle}_\phi$ as the MSD in the base mechanical trajectory with COM displacement-corrected end time coordinates, $\widetilde{\langle r^2(\theta)\rangle}_\phi = \langle r^2(\theta)\rangle_\phi - \delta^2{}_{\text{COM}}(\theta)$, then the MSD in the looped mechanical trajectory can be approximated as

$$\langle r^2(t)\rangle_\phi \approx \frac{t}{\theta}\times\widetilde{\langle r^2(\theta)\rangle}_\phi + \left\lfloor\frac{t}{\theta}\right\rfloor\times\langle r^2\rangle_\phi^{\text{join}} + \left\lfloor\frac{t}{\theta}\right\rfloor^2\times\delta^2{}_{\text{COM}}(\theta).$$

After multiple joins, on timescales that are much longer than the reactor-scale Brownian time, the influence of the COM drift on MSD may be significant [see Fig. 3(d), solid lines]. If from obtained MSDs one subtracts the respective expected contribution of the COM drift (calculated separately

for each base mechanical trajectory), a linear time dependence is recovered [Fig. 3(d), dashed lines]. It should be emphasized that a super-linear increase of MSD in not indicative of accelerating diffusion of molecules; their diffusive properties remain unchanged over time and the reaction kinetics, determined fully by the looped contacts sequence (Fig. 1), is unaffected.

C. Reaction kinetics in a monostable system

We consider a simple phosphorylation–dephosphorylation reaction cycle,

$$\mathcal{K} + \mathcal{S}_u \xrightarrow{k_0} \mathcal{K} + \mathcal{S}_p, \quad \mathcal{P} + \mathcal{S}_p \xrightarrow{q_0} \mathcal{P} + \mathcal{S}_u, \tag{1}$$

where $\mathcal{K}$ and $\mathcal{P}$ denote enzymes, kinase and phosphatase, and $\mathcal{S}_u$, $\mathcal{S}_p$ denote dephosphorylated and phosphorylated substrate molecules, respectively. This monostable reaction system has been studied in, e.g., Ref. [20], where it is demonstrated that the steady-state fraction of phosphorylated substrates can increase or decrease with diffusivity depending on relative concentrations of both enzymes. As in Ref. [20], we focus on the case when $\mathcal{K}$ are more abundant than $\mathcal{P}$ ($K = 10\,P$) and $\mathcal{K}$ are catalytically much less active than $\mathcal{P}$ ($q_0 = 100\,k_0$). In this case, the fraction of phosphorylated $\mathcal{S}$ markedly depends on the diffusion coefficient: at low diffusivity, $\mathcal{S}$ remain mostly in the phosphorylated state; at high diffusivity, $\mathcal{S}$ are mostly dephosphorylated.

The diffusion coefficient in the base mechanical trajectory cannot be changed; however, by scaling uniformly the rate constants of all chemical reactions within trajectory looping one can simulate the stochastic kinetics in either reaction-controlled or diffusion-controlled regime. When the average distance traveled by a phosphorylated substrate until dephosphorylation (Kuramoto correlation length), $\sqrt{D_0/q_0}$, is larger than the diameter of the reactor, L, then the chemical reactor shall be considered well mixed. Henceforth, we assume that the dephosphorylation reaction rate $q_0 = \lambda/\tau_B$ sets the time scale of chemical processes, that is, all other chemical rates are defined relative to q_0. Since propensities of reactions are proportional to λ, decreasing λ is equivalent to simultaneously increasing diffusivity and lengthening the time scale.

In Fig. 4(a) we demonstrate that the equilibration kinetics of the monostable system, Eq. (1), simulated within trajectory looping in the reaction-controlled regime (in the well-mixed reactor) matches very well the equilibration kinetics simulated according to the Gillespie algorithm with both bimolecular reaction rates multiplied by χ/N. For parameter values assumed in Fig. 4, the reactor becomes well mixed for λ of order of 10^{-2}. For this λ, to reach the end time of $300\,q_0^{-1}$ in Fig. 4(a), the base contacts sequence of duration $\theta = 3\,\tau_B$ had to be used 10^4 times (for $\theta = 10\,\tau_B$, 3×10^3 times).

The intensity of reactions increases with λ and the system exhibits a gradual transition from the reaction-limited to the diffusion-limited regime, as demonstrated in Fig. 4(b). In the fast-diffusion regime, the fraction tends to $1/11$, whereas in the slow-diffusion regime, the fraction tends to $10/11$, in agreement with the results of [20]. For intermediate $\lambda = 10$ and 10^2, the fraction of phosphorylated substrates in Fig. 4(b) is slightly lower for $\theta = 3\,\tau_B$ than for $\theta = 10\,\tau_B$, which results from the fact that joins that are more frequent than for $\theta = 10\,\tau_B$ introduce additional mixing [as analyzed in Fig. 3(b)].

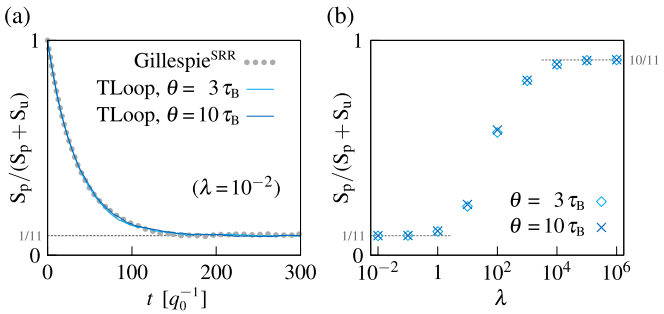

FIG. 4. Fraction of phosphorylated substrates, $S_p/(S_u + S_p)$, in the monostable reaction system Eq. (1). (a) Fraction of phosphorylated substrates in time. Initially, $S_p = S$ ($S_u = 0$). Two methods are used to simulate system equilibration: Gillespie algorithm with scaled reaction rates (Gillespie^{SRR}) and trajectory looping ("TLoop") with $\lambda = 10^{-2}$ applied to base mechanical trajectories of two different lengths, θ. Each curve results from averaging over three stochastic simulations. (b) Fraction of phosphorylated substrates in the steady state as a function of λ for base mechanical trajectories of different lengths, θ. In the fast-diffusion regime, the fraction tends to $1/11$, whereas in the slow-diffusion regime, the fraction tends to $10/11$ (both limits are marked with dashed lines). In both panels: $N = 3375$, $K = \lfloor 0.3\,N \rfloor$, $P = \lfloor 0.03\,N \rfloor$, $S = N - (K+P)$, $\phi = 0.2$ ($\chi \simeq 0.855$), $\epsilon = 0.05$, $\delta = 0.1$, $q_0 = \lambda/\tau_B$, $k_0 = 0.01\,q_0$.

D. State-to-state transition rates in a bistable system

Trajectory looping can be applied to enhance sampling of rare events in stochastic spatially extended systems. In this subsection we analyze events of switching between metastable states in a bistable reaction–diffusion system that has been analyzed previously by means of on-lattice kinetic Monte Carlo simulations in Ref. [21]. The system contains autophosphorylating bisphosphorylatable kinases $\mathcal{K}$ and phosphatases $\mathcal{P}$, that react as follows:

$$\mathcal{K}_u + \mathcal{K}_u \xrightarrow{2c_1} \mathcal{K}_u + \mathcal{K}_p, \quad \mathcal{K}_u + \mathcal{K}_p \xrightarrow{c_1} \mathcal{K}_u + \mathcal{K}_{pp}, \tag{2a}$$

$$\mathcal{K}_p + \mathcal{K}_u \xrightarrow{2c_2} \mathcal{K}_p + \mathcal{K}_p, \quad \mathcal{K}_p + \mathcal{K}_p \xrightarrow{c_2} \mathcal{K}_p + \mathcal{K}_{pp}, \tag{2b}$$

$$\mathcal{K}_{pp} + \mathcal{K}_u \xrightarrow{2c_3} \mathcal{K}_{pp} + \mathcal{K}_p, \quad \mathcal{K}_{pp} + \mathcal{K}_p \xrightarrow{c_3} \mathcal{K}_{pp} + \mathcal{K}_{pp}, \tag{2c}$$

$$\mathcal{P} + \mathcal{K}_{pp} \xrightarrow{2q_0} \mathcal{P} + \mathcal{K}_p, \quad \mathcal{P} + \mathcal{K}_p \xrightarrow{q_0} \mathcal{P} + \mathcal{K}_u. \tag{2d}$$

Stochastic kinetics of the system exhibits fast fluctuations in the vicinity of each of the metastable steady states and relatively infrequent switches between basins of attraction of these states, as shown in Fig. 5(a). Of note, the timescale associated with switching can be much longer than θ or the reactor-scale Brownian time. Trajectories of the system simulated with trajectory looping with a sufficiently small λ exhibit characteristic bimodal distribution of states, depicted in Fig. 5(b) (for $\lambda = 10^{-1}$ the system is effectively monostable). Stationary state distribution is sensitive to λ. For

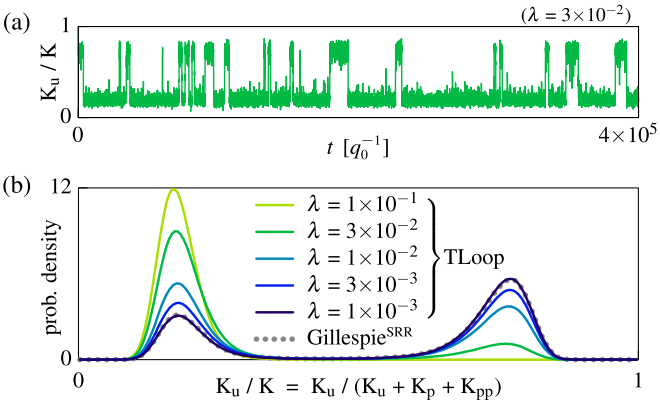

(c)

Simulation type	τ_{active} $[q_0^{-1}]$	τ_{inactive} $[q_0^{-1}]$
TLoop, $\lambda = 1\times10^{-1}$	$>100\times10^3$	0.3×10^3
TLoop, $\lambda = 3\times10^{-2}$	20×10^3	3.3×10^3
TLoop, $\lambda = 1\times10^{-2}$	8.5×10^3	7.4×10^3
TLoop, $\lambda = 3\times10^{-3}$	6.3×10^3	9.7×10^3
TLoop, $\lambda = 1\times10^{-3}$	5.4×10^3	12×10^3
Gillespie$^{\text{SRR}}$	5.7×10^3	12×10^3
Gillespie$^{\text{SRR}-0.1\%}$	5.0×10^3	13×10^3
Gillespie$^{\text{SRR}+0.1\%}$	6.4×10^3	11×10^3

FIG. 5. State-to-state transitions in the bistable reaction system (2). (a) Exemplary trajectory resulting from trajectory looping with $\lambda = 3\times10^{-2}$. (b) Comparison of the stationary probability distribution resulting from simulations with trajectory looping ("TLoop") for five values of λ and simulations according to the Gillespie algorithm with reaction rates scaled by the expected number of neighbors (superscript "SRR"). (c) Mean residence times in both metastables states, estimated based on 1000 transition events. Results from the Gillespie algorithm-based simulations, in which phosphorylation reaction rates are either decreased or increased by one per-mille, are denoted with superscripts "SRR−0.1%" and "SRR+0.1%," respectively. In all panels: $N = 500$, $\rho_{\mathcal{K}} = 0.8$, $\rho_{\mathcal{P}} = 0.2$, $K = \rho_{\mathcal{K}} N$, $P = \rho_{\mathcal{P}} N$, $\phi = 0.2$ ($\chi \simeq 0.855$), $\epsilon = 0.05$, $\delta = 0.1$, $\theta = 100\,\tau_{\text{B}}$, $q_0 = \lambda/\tau_{\text{B}}$, $c_1 = 0.025\,q_0$, $c_2 = 0.0075\,q_0$, $c_3 = q_0$.

$\lambda = 1\times10^{-3}$, when the system is well mixed, the distribution matches perfectly the distribution obtained from the Gillespie algorithm-based simulations with scaled reaction rates. The residence times or, equivalently, the mean first-passage times that correspond to distributions shown in Fig. 5(b), obtained each from at least 1000 switches, are contained in Fig. 5(c). Since in cellular biochemistry kinase phosphorylation is often associated with its activation, the state of low (high) number of $\mathcal{K}_{\text{u}}$ is referred to as the active (inactive) state. The ratio $\tau_{\text{active}}/(\tau_{\text{active}} + \tau_{\text{inactive}})$ is the same as the probability mass contained in the first peak of a respective bimodal distribution in Fig. 5(b). When in the Gillespie algorithm-based simulations the phosphorylation rates (c_1, c_2, and c_3) are either decreased or increased by just one per-mille (0.1%), τ_{active} and τ_{inactive} are noticeably different [Fig. 5(c)]. This, in addition to the match of probability distributions shown in Fig. 5(b), indicates that the well-mixed limit parameters can be reproduced by trajectory looping to a very high accuracy.

E. Traveling waves in a bistable system

In spatially extended domains, the stochastic bistable reaction–diffusion system, Eq. (2), admits traveling wave solutions. In the mean-field limit, the evolution of the normalized kinase species concentrations $k_{\text{u}}, k_{\text{p}}$, and k_{pp} (where $k_{\text{u}} + k_{\text{p}} + k_{\text{pp}} = 1$) is governed by the system of partial differential equations (PDEs):

$$\frac{\partial k_{\text{u}}}{\partial t} = D\nabla^2 k_{\text{u}} + Q_0 k_{\text{p}} - 2(C_1 k_{\text{u}} + C_2 k_{\text{p}} + C_3 k_{\text{pp}})k_{\text{u}}, \quad (3a)$$

$$\frac{\partial k_{\text{p}}}{\partial t} = D\nabla^2 k_{\text{p}} + 2(C_1 k_{\text{u}} + C_2 k_{\text{p}} + C_3 k_{\text{pp}})k_{\text{u}} + 2Q_0 k_{\text{pp}} - (C_1 k_{\text{u}} + C_2 k_{\text{p}} + C_3 k_{\text{pp}})k_{\text{p}} - Q_0 k_{\text{p}}, \quad (3b)$$

$$\frac{\partial k_{\text{pp}}}{\partial t} = D\nabla^2 k_{\text{pp}} + (C_1 k_{\text{u}} + C_2 k_{\text{p}} + C_3 k_{\text{pp}})k_{\text{p}} - 2Q_0 k_{\text{pp}}, \quad (3c)$$

where the diffusion coefficient D is equal to that of the spatial stochastic system for the appropriate volume fraction. Reaction rate coefficients C_i and Q_0 are related to the original coefficients c_i and q_0 as follows: $C_i = (K/N)\chi c_i$ and $Q_0 = (P/N)\chi q_0$, where N is the total number of molecules, K is the number of kinases, and P is the number of phosphatases. To obtain traveling wave solutions to Eqs. (3), we assume that the functions k_{u}, k_{p}, and k_{pp} depend only on time and one spatial variable z, and start from initial condition in which for $z < 0$ the system assumes one of two stable states, whereas for $z \geqslant 0$ it assumes the other.

We performed simulations of the spatial stochastic model within trajectory looping using the base mechanical trajectory of length $\theta = 10\,\tau_{\text{B}}$ in an elongated domain that contained $N = 5000$ molecules at the volume fraction $\phi = 0.2$. The simulations started from the initial condition [Fig. 6(a)] in which the whole domain is in the inactive stationary state (high fraction of $\mathcal{K}_{\text{u}}$) except for a stretch of length of 10% of the domain, which is in the active state (low fraction of $\mathcal{K}_{\text{u}}$). Propagation of (stochastic) activating traveling wave implies that the area occupied by the active state increases (approximately) linearly with time as $2v \times t$, where v is the propagation velocity; coefficient 2 arises from the fact that the traveling wave propagates in both directions. As a result, the fraction of $\mathcal{K}_{\text{u}}$ averaged over the whole domain, $f_{\text{u}}(t)$, decreases linearly with time [Fig. 6(b)]: $df_{\text{u}}/dt = 2v(f_{\text{u}}^{\text{active}} - f_{\text{u}}^{\text{inactive}})/\ell$, where $f_{\text{u}}^{\text{active}}$ and $f_{\text{u}}^{\text{inactive}}$ denote the value of f_{u} in the active state and in the inactive state, respectively, and ℓ is the length of the domain. Based on the above formula we can calculate the traveling wave velocity as

$$v = \frac{df_{\text{u}}}{dt}\frac{\ell}{2\left(f_{\text{u}}^{\text{active}} - f_{\text{u}}^{\text{inactive}}\right)}. \quad (4)$$

To estimate $v(\lambda)$ numerically, for each λ we performed 20 simulations and based on the profiles of $f_{\text{u}}^{\text{inactive}}(t)$ we estimated df_{u}/dt. In Fig. 6(c) we show that these estimates are in agreement with the values obtained from numerical solutions of Eqs. (3) in Matlab (The MathWorks, Inc., USA).

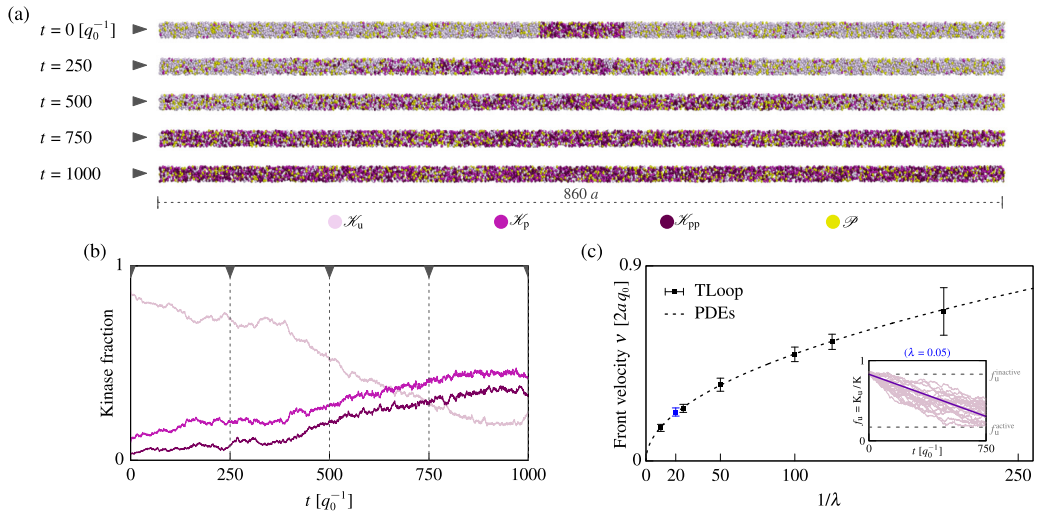

FIG. 6. Stochastic traveling wave in the bistable system (2). (a) Five snapshots from the trajectory of a propagating wavefront. Simulation parameters for the base mechanical trajectory are: $N = 5000$, $\phi = 0.2$, $\theta = 10\tau_B$, and $\epsilon = 0.1$. Simulation was performed in the box of the dimensions ratio 1:1:78 and length $\ell = 860a$ with periodic boundary conditions in three directions. Simulation parameters for chemical reactions are: $q_0 = \lambda/\tau_B$, $c_1 = 0.005\,q_0$, $c_2 = 0.038\,q_0$, $c_3 = q_0$, $K = 0.8\,N$, $P = 0.2\,N$, $\lambda = 0.05$. (b) Fractions of kinase species in time. (c) Wavefront propagation velocity as a function of λ. Insert shows results of 20 simulations (all for $\lambda = 0.05$) used to estimate df_u/dt. The error bars represent the standard error of the mean.

III. DISCUSSION

Systems of coupled biochemical reactions which underlie cellular regulatory processes often have two or more steady states associated with cell physiological outcomes [22–24]. Noise—inherent in biochemical systems—allows for transitions between these states [25,26]. The transitions can however be notoriously rare: biochemically implemented genetic switch in phage λ requires millions of generations to switch on the lytic pathway [27]. Since transition times are typically much longer than relaxation times of monostable biochemical systems, sampling of transition events in spatially extended systems by means of direct simulations is computationally very demanding.

Chemical kinetics in spatially extended stochastic systems strongly depends on the diffusivity of substrates. While in well-mixed systems time to a stochastic transition grows exponentially with the size of the system [28], spatially extended systems at a small diffusivity have their transition rates very different from those of the corresponding systems in the well-mixed limit. This is because for slow diffusion the state-to-state transitions can be achieved by means of a local transition that initiates a traveling wave [1] which then drives the whole reactor towards the "more stable" steady state [29]. Even though the expected time for nucleation of the wave is much shorter than the time necessary for a simultaneous switch of the whole domain, both timescales may be orders of magnitude longer than time required by a molecule to cover a distance comparable to the reactor diameter.

Trajectory looping is capable of reaching simulated times orders of magnitude longer than the simulated length of base mechanical trajectory, significantly enhancing the sampling of rare events. Assuming that τ_B of a protein molecule in a signaling system is of order of 10^{-6} s of real time (as can be estimated based on, e.g., Ref. [30]), simulated time required to estimate transition times in the analyzed bistable system for $\lambda = 10^{-2}$ should be of order of an hour. The trajectory looping algorithm is thus suitable for simulating reaction–diffusion systems on the physiologically relevant timescales at the single-molecule resolution. The method is independent of the numerical scheme used to obtain the underlying base mechanical trajectory; it can be applied equally well to mechanical trajectories with or without hydrodynamic interactions.

We verified the accuracy of the proposed method in three cases: (i) in the limits of fast and slow diffusion, by comparing simulated steady state values of monostable system with an analytical prediction; (ii) in the limit of fast diffusion, by comparing trajectory looping simulations with those obtained using Gillespie algorithm; (iii) in the elongated domains, we reproduced traveling wave solutions, and showed that the wavefronts propagate with the average velocity consistent with that predicted by numerical solutions of the corresponding system of PDEs. Since the trajectory looping algorithm benefits from reusing multiple times the same base mechanical trajectory, the number of molecules in the simulated system cannot change. Such systems are common in models of cellular signal transduction pathways that are based on reversible covalent substrate modifications, such as phosphorylation, ubiquitination, or acetylation.

In addition to the problems analyzed in this article, we expect that trajectory looping can be applicable to capture and characterize other behaviors and properties that can be hardly observable in spatial stochastic simulations such as the range of a homoclinic traveling wave, time to extinction of an oscillating system, or synchronization of oscillators (both in systems with a limit cycle). Exemplary bimolecular reaction systems that are extensions of system Eq. (2) and allow for either a homoclinic traveling wave or a limit-cycle oscillations are provided in the Appendix.

TABLE I. Computational cost associated with key procedures used to perform simulations with and without looping. Computational complexity of obtaining the base mechanical trajectory depends on the underlying method and may vary from $\mathcal{O}(N)$ for cell list-based approaches to $\mathcal{O}(N^3)$ in the case of simulations that include, e.g., hydrodynamic interactions. The last column contains single-core processor times and the number of calls to a given procedure in the case of a trajectory looping-based simulation.

Procedure	Number of calls		Complexity	CPU time for Fig. 5 ($\lambda = 10^{-2}$)
	without looping	with looping		
Base mechanical trajectory (of length θ)	K	1	$\mathcal{O}(N)$ to $\mathcal{O}(N^3)$	3 h ($\times 1$)
Base contacts sequence	K	1	$\mathcal{O}(N^2)$	1 min ($\times 1$)
Assignment (Hungarian algorithm)	0	K	$\mathcal{O}(N^3)$	10^{-2} s ($\times K$)
Chemical trajectory (within θ)	K	K	$\mathcal{O}(N)$	1 s ($\times K$)

IV. METHODS

A. Brownian dynamics simulation

The algorithm of trajectory looping is described in detail in the first subsection of the Results section. The base mechanical trajectory, which is an input to trajectory looping, is obtained independently. Below we describe the method for obtaining the base mechanical trajectories used in simulations reported in this article.

Base mechanical trajectories were generated using standard Brownian dynamics simulations of N identical molecules. The volume V of the simulation box was set to match the required volume fraction $\phi = N \times v/V$, where $v = (4/3)\pi a^3$ is the single-molecule volume. In both cubic and elongated cuboidal boxes, periodic boundary conditions were assumed at all boundaries. Average distance traveled by a molecule in a single simulation time step Δt is of order of $\sqrt{\Delta t \times D_0}$. To set the time step we compare this distance with characteristic surface-to-surface distance between molecules, $d_{ss} = (V/N)^{1/3} - 2a$, which is the distance between surfaces of neighboring molecules arranged in a cubic lattice at a given ϕ. To this end, we introduce parameter ϵ and set $\Delta t = (\epsilon \times d_{ss})^2/D_0$. In all simulations $\epsilon \times d_{ss} < \delta$, which makes the probability of omitting a reaction event low.

Molecules interact with a hard-sphere potential ensuring perfectly elastic collisions [31,32]. In every time step, potential random displacements of all molecules are calculated with zero mean and the variance equal $\langle r^2(\tau = \Delta t)\rangle_0 = 6D_0 \times \Delta t$. Based on initial molecule positions and velocities calculated from the displacements, a list of collisions is created. If there are no collisions, molecules are moved directly to their target locations. If the list of colliding molecules is nonempty, molecules are moved with constant velocities until a first collision. Upon a collision, positions and velocities of the colliding molecules and the list of all further collisions are updated. Due to the presence of other molecules in the simulation box, the mean square displacement of a molecule in the base mechanical trajectory of duration θ, $\langle r^2(\tau = \theta)\rangle_\phi = \sum_{i=1}^{N} |\vec{R}_i(\theta) - \vec{R}_i(0)|^2/N$, is smaller than $\langle r^2(\tau = \theta)\rangle_0 = (M-1) \times \langle r^2(\tau = \Delta t)\rangle_0$.

B. Simulation times

A detailed digest of computational cost of the procedures used to generate the key data structures present in Fig. 1 is provided in Table I. Generation of the base mechanical trajectory that was used to estimate probability density distribution in the bistable reaction system, Eq. (2), presented in Fig. 5(b), required about 3 h of a single-core processor. At $\lambda = 10^{-2}$, simulation time of the base mechanical trajectory is $\theta = 1\,[q_0^{-1}]$, whereas simulation time to observe 1000 switches that were used to estimate both τ_{active} and $\tau_{inactive}$ [Fig. 5(c)] is $1000 \times (8.5 + 7.4) \times 10^3 \simeq 1.6 \times 10^7\,[q_0^{-1}]$, which means that within trajectory looping the base mechanical trajectory was reused $K = 1.6 \times 10^7$ times. Single-core processor time to obtain the looped chemical trajectory (see Table I for processor times of individual procedures) was 3 h + 1 min + $K \times (10^{-2}\text{ s} + 0.5\text{ s}) \simeq 3$ months (in practice, the simulations were performed in parallel on a computer cluster, so this is an aggregate real time). In a direct, naive approach without trajectory looping, in which diffusive steps are interleaved with simulation of chemical reactions, single-core processor time to obtain equally long chemical trajectory could be estimated (see Table I) as $K \times (3\text{ h} + 1\text{ min} + 0.5\text{ s})$, which amounts to more than 5000 years.

We should notice that simulation of the trajectory used to estimate probability density distribution for the same reaction system Eq. (2) [dotted line in Fig. 5(b)], but without spatial resolution (i.e., under the assumption that the system is perfectly mixed) using Gillespie algorithm takes only 5 min.

ACKNOWLEDGMENTS

Numerical codes used to generate base mechanical trajectories were written by late Prof. Eligiusz Wajnryb. Simulations were performed using computational resources of ACK Cyfronet AGH cluster Prometheus (within the PL-grid infrastructure) and the Della cluster of the Princeton University. P.J.Z. was supported by the Polish Ministry of Science and Higher Education ("Mobility Plus" Project No. 1294/MOB/IV/2015/0). T.L. acknowledges support from the National Science Centre (NCN), Poland (Grant No. 2014/14/M/NZ6/00537).

P.J.Z. and M.K. contributed equally to this work.

APPENDIX: EXTENDED BIMOLECULAR REACTION SYSTEM

When the system Eq. (2) is amended with an additional mechanism of inactivation of kinases $\mathcal{K}$, mediated by a $\mathcal{K}$-phosphorylatable inhibitor $\mathcal{I}$ that shares phosphatase $\mathcal{P}$ with

kinases $\mathcal{K}$:

$$\mathcal{K}_{pp} + \mathcal{I}_u \xrightarrow{2c_4} \mathcal{K}_{pp} + \mathcal{I}_p, \tag{A1a}$$

$$\mathcal{K}_{pp} + \mathcal{I}_p \xrightarrow{c_4} \mathcal{K}_{pp} + \mathcal{I}_{pp}, \tag{A1b}$$

$$\mathcal{I}_{pp} + \mathcal{K}_{pp} \xrightarrow{2c_5} \mathcal{I}_{pp} + \mathcal{K}_p, \tag{A1c}$$

$$\mathcal{I}_{pp} + \mathcal{K}_p \xrightarrow{c_5} \mathcal{I}_{pp} + \mathcal{K}_u, \tag{A1d}$$

then the corresponding system of PDEs:

$$\frac{\partial k_u}{\partial t} = D\nabla^2 k_u + (Q_0 + C_5 i_{pp})k_p - 2(C_1 k_u + C_2 k_p + C_3 k_{pp})k_u, \tag{A2a}$$

$$\frac{\partial k_p}{\partial t} = D\nabla^2 k_p + 2(C_1 k_u + C_2 k_p + C_3 k_{pp})k_u + 2(Q_0 + C_5 i_{pp})k_{pp} - (C_1 k_u + C_2 k_p + C_3 k_{pp})k_p - (Q_0 + C_5 i_{pp})k_p \tag{A2b}$$

$$\frac{\partial k_{pp}}{\partial t} = D\nabla^2 k_{pp} + (C_1 k_u + C_2 k_p + C_3 k_{pp})k_p - 2(Q_0 + C_5 i_{pp})k_{pp}, \tag{A2c}$$

$$\frac{\partial i_u}{\partial t} = D\nabla^2 i_u - 2C_4 k_{pp} i_u + Q_1 i_p, \tag{A2d}$$

$$\frac{\partial i_p}{\partial t} = D\nabla^2 i_p + 2C_4 k_{pp} i_u + 2Q_1 i_{pp} - (Q_1 + C_4 k_{pp})i_p, \tag{A2e}$$

$$\frac{\partial i_{pp}}{\partial t} = D\nabla^2 i_{pp} - 2Q_1 i_{pp} + K_4 k_{pp} i_p, \tag{A2f}$$

exhibits excitable (traveling pulse) dynamics for parameter values:

$$Q_0 = 1,$$
$$C_1 = 0.02,$$
$$C_2 = 0.2,$$
$$C_3 = 4,$$
$$C_4 = 0.03,$$
$$C_5 = 1,$$
$$Q_1 = 0.003,$$
$$D = 0.1$$

and limit-cycle oscillations for parameter values:

$$Q_0 = 1,$$
$$C_1 = 3{\times}0.02,$$
$$C_2 = 3{\times}0.2,$$
$$C_3 = 3{\times}4,$$
$$C_4 = 10{\times}0.03,$$
$$C_5 = 10{\times}1,$$
$$Q_1 = 10{\times}0.003,$$
$$D = 0.1.$$

[1] J. Keener and J. Sneyd, *Mathematical Physiology* (Springer, New York, 1998).

[2] T. Ando and J. Skolnick, Crowding and hydrodynamic interactions likely dominate *in vivo* macromolecular motion, Proc. Natl Acad. Sci. USA **107**, 18457 (2010).

[3] D. T. Gillespie, Exact stochastic simulation of coupled chemical reactions, J. Phys. Chem. **81**, 2340 (1977).

[4] R. M. Donovan, J.-J. Tapia, D. P. Sullivan, J. R. Faeder, R. F. Murphy, M. Dittrich, and D. M. Zuckerman, Unbiased rare event sampling in spatial stochastic systems biology models using a weighted ensemble of trajectories, PLOS Comput. Biol. **12**, e1004611 (2016).

[5] H. Kuwahara and I. Mura, An efficient and exact stochastic simulation method to analyze rare events in biochemical systems, J. Chem. Phys **129**, 165101 (2008).

[6] C. Dellago, P. G. Bolhuis, F. S. Csajka, and D. Chandler, Transition path sampling and the calculation of rate constants, J. Chem. Phys. **108**, 1964 (1998).

[7] R. J. Allen, P. B. Warren, and P. R. ten Wolde, Sampling Rare Switching Events in Biochemical Networks, Phys. Rev. Lett. **94**, 018104 (2005).

[8] J. Elf and M. Ehrenberg, Spontaneous separation of bi-stable biochemical systems into spatial domains of opposite phases, Syst. Biol. **1**, 230 (2004).

[9] J. S. van Zon and P. R. ten Wolde, Simulating Biochemical Networks at the Particle Level and in Time and Space: Green's Function Reaction Dynamics, Phys. Rev. Lett. **94**, 128103 (2005).

[10] K. Takahashi, S. Tănase-Nicola, and P. R. ten Wolde, Spatio-temporal correlations can drastically change the response of a MAPK pathway, Proc. Natl Acad. Sci. USA **107**, 2473 (2010).

[11] G. A. Bird, *Molecular Gas Dynamics and the Direct Simulation of Gas Flows* (Clarendon Press, Oxford, 1994).

[12] P. Dziekan, A. Lemarchand, and B. Nowakowski, Particle dynamics simulations of Turing patterns, J. Chem. Phys **137**, 074107 (2012).

[13] J. Das, M. Kardar, and A. K. Chakraborty, Positive feedback regulation results in spatial clustering and fast spreading of active signaling molecules on a cell membrane, J. Chem. Phys. **130**, 245102 (2009).

[14] B. N. Kholodenko, J. F. Hancock, and W. Kolch, Signalling ballet in space and time, Nat. Rev. Mol. Cell. Biol. **11**, 414 (2010).

[15] H. W. Kuhn, The Hungarian method for the assignment problem, Nav. Res. Logist. Q. **2**, 83 (1955).

[16] J. Munkres, Algorithms for the assignment and transportation problems, J. Soc. Ind. Appl. Math. **5**, 32 (1957).

[17] D. E. King, Dlib-ml: A machine learning toolkit, J. Mach. Learn. Res. **10**, 1755 (2009), DLIB webpage: http://dlib.net.

[18] M. S. Wertheim, Exact Solution of the Percus–Yevick Integral Equation for Hard Spheres, Phys. Rev. Lett. **10**, 321 (1963).

[19] LOOPER webpage: http://pmbm.ippt.pan.pl/software/looping.

[20] P. Szymańska, M. Kochańczyk, J. Miękisz, and T. Lipniacki, Effective reaction rates in diffusion-limited phosphorylation–dephosphorylation cycles, Phys. Rev. E **91**, 022702 (2015).

[21] M. Kochańczyk, J. Jaruszewicz, and T. Lipniacki, Stochastic transitions in a bistable reaction system on the membrane, J. R. Soc. Interface **10**, 20130151 (2013).

[22] T. S. Gardner, C. R. Cantor, and J. J. Collins, Construction of a genetic toggle switch in *Escherichia coli*, Nature **403**, 339 (2000).

[23] S. Huang, G. Eichler, Y. Bar-Yam, and D. E. Ingber, Cell Fates as High-Dimensional Attractor States of a Complex Gene Regulatory Network, Phys. Rev. Lett. **94**, 128701 (2005).

[24] M. Lu, M. K. Jolly, H. Levine, J. N. Onuchic, and E. Ben-Jacob, MicroRNA-based regulation of epithelial–hybrid–mesenchymal fate determination, Proc. Natl Acad. Sci. USA **110**, 18144 (2013).

[25] M. Kærn, T. C. Elston, W. J. Blake, and J. J. Collins, Stochasticity in gene expression: from theories to phenotypes, Nat. Rev. Genet. **6**, 451 (2005).

[26] H. Maamar, A. Raj, and D. Dubnau, Noise in gene expression determines cell fate in Bacillus subtilis, Science **317**, 526 (2007).

[27] J. W. Little and C. B. Michalowski, Stability and instability in the lysogenic state of phage lambda, J. Bacteriol. **192**, 6064 (2010).

[28] S. Redner, *A Guide to First-Passage Processes* (Cambridge University Press, New York, NY, 2001).

[29] P. J. Zuk, M. Kochańczyk, J. Jaruszewicz, W. Bednorz, and T. Lipniacki, Dynamics of a stochastic spatially extended system predicted by comparing deterministic and stochastic attractors of the corresponding birth–death process, Phys. Biol. **9**, 055002 (2012).

[30] T. Kalwarczyk, M. Tabaka, and R. Hołyst, Biologistics—Diffusion coefficients for complete proteome of *Escherichia coli*, Bioinformatics **28**, 2971 (2012).

[31] B. J. Alder and T. E. Wainwright, Studies in molecular dynamics. I. General method, J. Chem. Phys. **31**, 459 (1959).

[32] A. J. C. Ladd, Dynamical simulations of sedimenting spheres, Phys. Fluids A **5**, 299 (1993).